Hyphae Detection in Fungal Keratitis Images With Adaptive Robust Binary Pattern

**XUELIAN WU[1], QINGCHEN QIU[1], ZHI LIU[1], (Member, IEEE), YUEFENG ZHAO[2],
BIN ZHANG[3], YONG ZHANG[4], XINYI WU[1], AND JIANMIN REN[1]**
[1]Shandong University, Jinan 250100, China
[2]School of Physics and Electronics, Shandong Normal University, Jinan 250100, China
[3]Shandong Provincial Maternity and Child Care Hospital, Jinan 250100, China
[4]Shandong Provincial Hospital of Ophthalmology, Jinan 250100, China

Corresponding author: Zhi Liu (liuzhi@sdu.edu.cn)

ABSTRACT Fungal keratitis is an inflammation of the cornea that results from infection by fungal organisms. It has a high rate of blindness, which makes the accurate diagnosis of fungal keratitis important. Confocal microscopy is an optical imaging technique that assists doctors in diagnosing fungal keratitis, and cornea images obtained by confocal microscopy can be used to detect hyphae. The current challenges are how to classify normal cornea images with nerves and abnormal cornea images with hyphae and how to detect the hyphae in a complicated background. To address this problem, this paper proposes a novel automatic hyphae detection method that assists doctors in making diagnoses. It includes two primary steps: texture classification of images and hyphae detection. In texture classification step, first, after image enhancement using a subregional contrast stretching algorithm, an adaptive robust binary pattern (ARBP), which is an improvement on the adaptive median binary pattern (AMBP), is proposed and adopted to extract texture features; and a support vector machine model is used to classify the normal and abnormal images. In the hyphae detection step, binarization and a connected domain process are used to further enhance the targets, and a line segment detector algorithm is adopted to detect the hyphae; then, the hyphal density is defined to quantitatively evaluate the infection severity. The contributions of this study include the improvement of the AMBP and the design of a novel framework. ARBP can extract effective texture features of images with relatively bright and small targets. The experimental results demonstrate the effectiveness of the proposed framework.

INDEX TERMS Fungal keratitis, texture analysis, ARBP, LSD, SVM.

I. INTRODUCTION

Fungal keratitis [1] is an inflammation of the cornea that results from infection by a fungal organism. The lack of rapid and effective early diagnostic methods often leads to early misdiagnosis and delayed disease treatment, which cause serious complications such as corneal perforation, anterior chamber empyema, endophthalmitis and blindness. Because the incidence has increased in recent years [2], the early diagnosis and accurate treatment of fungal keratitis are especially important.

The primary diagnostic methods of fungal keratitis include slit-lamp examination, microscopic examination of cornea scrapings, fungal culture, tissue biopsy, polymerase chain reaction (PCR) and confocal microscopy [3]. These methods

are widely used clinically with good results but have shortcomings. For example, slit-lamp examination can only help doctors observe symptoms and determine simple and tentative diagnoses; microscopic examination of cornea scrapings and tissue biopsy could cause secondary damage to the corneal tissue of a patient; fungal culture takes a relatively long time, leading to difficulties in real-time diagnosis [4], [5]; and the cost of PCR is high [6]. Among the various diagnostic methods, confocal microscopy [7], an optical imaging technique that relies on a spatial pinhole placed at the confocal plane of the lens to eliminate out-of-focus light, has many advantages in the diagnosis of fungal keratitis. Confocal microscopy is emerging as a clinically important noninvasive and non-contacting instrument for the diagnosis

and management of keratitis with a high positive rate. It allows for in vivo identification of filamentous structures that are morphologically consistent with fungus in an area of stromal infiltration, which relies on the subjective judgment of doctors [8].

The cornea image obtained by confocal microscopy can also be used to diagnose fungal keratitis at a cellular level. The detection of hyphae in a cornea image is crucial evidence of a fungal keratitis infection because there are no hyphae in normal cornea fundus images, and the diagnosis is primarily based on the number and morphology of the observed hyphae. Examples of normal cornea images with nerves and abnormal cornea images with hyphae are shown in Fig. 1. Considering that hyphae from infected cornea and nerves from healthy cornea are also threadlike, separating and detecting hyphae from nerves is an essential problem [9]. Experienced doctors can observe medical images and make an accurate diagnosis, but because of the large number of patients and images, the lack of excellent doctors in some areas and the subjective errors of doctors, an automatic hyphae detection method is needed. However, to date, little work has been done on the automatic detection of hyphae.
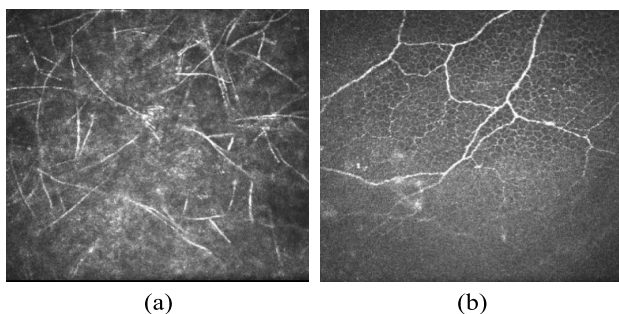

(a)   (b)

FIGURE 1. **(a) Normal cornea image with nerves obtained by Heidelberg Engineering HRT-3 confocal microscopy. (b) Abnormal cornea cornea image with hyphae obtained by Heidelberg Engineering HRT-3 confocal microscopy.**

Currently, the development of interdisciplinary approaches is becoming one of the trends of modern science and technology. Image analysis and processing, which is a rapidly developing discipline, also has an increasing number of excellent applications in the medical domain. Our team has introduced image analysis and processing techniques, specifically texture analysis [10], [11], into the diagnosis of fungal keratitis. Texture is an attribute of images that describes the variation and repetition of gray levels. Texture analysis extracts texture features through a texture descriptor, including the gray level co-occurrence matrix (GLCM) [12], [13], Gabor filter [14], local binary pattern (LBP) [15], [16], median binary pattern (MBP) [17], adaptive median binary pattern (AMBP) [18], [19].

Qiu *et al.* [9] have proposed an automatic hyphae image detection method in 2016 based on LBP and support vector machine (SVM) [20] model that can separate abnormal images from normal images with 93.53% accuracy.

However, it applies a fairly basic texture descriptor, LBP, to extract the features, which misses important texture information and negatively affects the classification results. Furthermore, it cannot detect or quantitatively evaluate hyphae.

In this paper, a novel framework that includes a new texture descriptor is proposed, and hyphae detection and quantitative evaluation are realized. The novel framework includes two primary steps: texture classification of images and hyphae detection. In texture classification step, firstly, we enhance the images using a sub-regional contrast stretching algorithm; then we propose an adaptive robust binary pattern (ARBP) to extract texture features; at last we adopt SVM model to classify the normal and abnormal images. In hyphae detection step, we apply binarization and a connected domain process to further enhance the target; then a line segment detector (LSD) algorithm is adopted to detect the hyphae; lastly the hyphal density is defined to quantitatively evaluate the infection severity. The novel automatic hyphae detection framework is shown in Fig. 2.
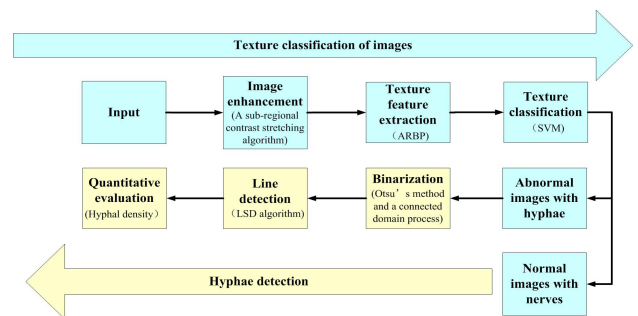

FIGURE 2. **The novel automatic hyphae detection framework.**

The contributions of this study include:

- The newly proposed texture analysis method ARBP. Considering that the brightness of the hyphae and nerves is higher than that of the background, we improve the AMBP by adding the average pixel value of the analysis window as a new parameter. ARBP can extract effective texture features of images with relatively bright and small targets.
- The design of the novel automatic hyphae detection framework. The experimental results demonstrate the effectiveness of the proposed framework.

The rest of paper is organized as follows. Section II introduces the related work on recent medical applications of texture analysis. In section III, several general texture analysis methods are introduced, then we propose a new texture analysis method ARBP and introduce the chosen classifier SVM, finally, the concrete framework of classification in this work is presented. Hyphae detection using a LSD method and quantitative evaluation are described in section VI. Section V demonstrates the experimental results and analysis. Finally, the conclusions and future research are summarized in section VI.

II. RELATED WORK

Recently, traditional medical diagnostic methods, such as slit-lamp examination, microscopic examination of cornea scrapings, fungal culture, tissue biopsy, PCR and confocal microscopy, still dominate the diagnosis of fungal keratitis. Although little research work has been done on the automatic detection of hyphae in cornea image, image analysis and processing, especially texture analysis, has been increasingly introduced to medical domain. Texture analysis [10], [11] methods in medical domain can approximately be classified into three categories: statistical methods, model based methods and spectral methods. In this section, some of the recent medical applications of texture analysis are described.

Statistical methods describe the statistical features of local area based on the gray value of pixels and its neighbors. Statistical features include the first-order statistics, the second-order statistics and the higher-order statistics. GLCM, which is one of the typical statistical texture analysis methods, has been applied in medical image analysis effectively. For example, Gaike *et al.* [21] proposed a novel third order GLCM features and observed the results in recognition of malignancy in a novel breast mammogram's regional database. Rohini and Soma [22] proposed a unique system in skin melanoma detection relies on harlick GLCM.

Model based methods describe texture based on certain mathematical models, a texture image is modeled as a probability model or as a linear combination of a set of basis function. Model based methods include Markov random fields (MRF), Wold model, etc. Rastghalam and Pourghassem [23] proposed a breast cancer detection algorithm using a novel MRF-based probable texture feature. Ahmadvand and Daliri [24] improved a rontime of MRF based method for Magnetic Resonance Imaging brain segmentation.

Spectral methods convert image data to frequency domain to extract the frequency domain features. Typical spectral methods include Fourier transform, wavelet transform, etc. Zou *et al.* [25] proposed to use the wavelet leader transform for studying trabecular bone patterns, experimental results on a recently released benchmark dataset show that wavelet leader transform boosts the performance of baseline wavelet transform by 5% in average. Virmani [26] investigated various wavelet-based texture descriptors for breast tissue density classification on MIAS dataset.

III. CLASSIFICATION OF CORNEA IMAGES

In this section, the general local texture descriptors, such as GLCM, Gabor filter, LBP, MBP and AMBP, are first introduced. Second, we propose a novel texture analysis method called ARBP, which is an improvement on AMBP. Then, the principle of classifier SVM performed in this work is presented. Finally, we introduce the classification framework for cornea images.

A. GENERAL TEXTURE ANALYSIS METHOD

1) GRAY LEVEL CO-OCCURRENCE MATRIX

GLCM [12], [13] is defined as a co-occurrence matrix or a co-occurrence distribution. In a gray-level image, a certain gray relationship, known as image gray-scale spatial correlation, exists among the pixels through the study of spatial gray level correlations to describe the texture.

GLCM can be presented as the following probability function:

$$p(i, j) = \frac{P(i, j | d, \theta)}{N} \quad (1)$$

where d is the interpixel distance, θ is the orientation, usually, $\theta = [0°, 45°, 90°, 135°]$, and N is the total number of possible outcomes.

Generally, we do not apply $p(i, j)$ directly, instead, we use GLCM statistical features which can realize satisfactory texture discrimination. General GLCM statistic features are defined as follows:

Angular second moment (energy):

$$ASM = \sum_{i=0}^{G-1} \sum_{j=0}^{G-1} [p(i, j)]^2 \quad (2)$$

Contrast:

$$Con = \sum_{i}^{G-1} \sum_{j}^{G-1} (i - j)^2 P(i, j) \quad (3)$$

Entropy:

$$Ent = -\sum_{i}^{G-1} \sum_{j}^{G-1} p(i, j) \log p(i, j) \quad (4)$$

Absolute value:

$$abs = \sum_{i=0}^{G-1} \sum_{j=0}^{G-1} |i - j| p(i, j) \quad (5)$$

2) GABOR FILTER

Gabor filter is a linear filter that is used in texture analysis, which can extract related features from different directions and on different scales in the frequency domain. The frequency and direction of Gabor filter are similar to those of the human vision system.

The two-dimensional Gabor filter [14] is a Gaussian nuclear function that is modulated by a sine wave, and it can be defined as follows:

$$g(x, y) = (\frac{1}{2\pi \sigma_x \sigma_y}) \exp(-\frac{1}{2}(\frac{x^2}{\sigma_x^2} + \frac{y^2}{\sigma_y^2}) + 2\pi j W_x) \quad (6)$$

where W is the modulation frequency, and σ_x and σ_y represent the spatial extent and frequency bandwidth of the Gabor filter, respectively.

A set of Gabor functions $g_{m,n}(x, y)$ can be obtained by a generating function with the mother-generating function $g(x, y)$.

$$g_{m,n}(x, y) = a^{-2m} g(x', y') \quad (7)$$

where $x' = a^{-m}(x \cos\theta_n + y \sin\theta_n)$, $y' = a^{-m}(-x \sin\theta_n + y \cos\theta_n)$, $\theta_n = n\pi/K$, and $a > 1$. Here, $m = 1, 2, \ldots M$ represents the number of scales, and $n = 1, 2 \ldots N$ represents the number of orientations.

For an $a * b$ size input image, the result after the Gabor wavelet transform can be written as follows:

$$G_{mn}(x, y) = \sum_{x_1} \sum_{y_1} I(x_1, y_1)g_{m,n}(x - x_1, y - y_1) \quad (8)$$

The mean deviation and standard deviation of the magnitude of the filtered images are used to represent the feature vectors that are used for classification [14].

3) LOCAL BINARY PATTERN

LBP [15], [16], which was proposed by Ojala et al., is a general local texture descriptor. It is a simple but powerful texture analysis method.

LBP can be defined in a 3×3 image patch. As shown in Fig. 3 and equation (9), it contains two main steps: a thresholding step and an encoding step. In the thresholding step, every pixel in the image patch is compared with the center pixel value, and then, it is converted to 0 or 1. This step aids in extracting the information of the local binary grayscale differences. In the encoding step, the resulting eight binary values are arranged as binary code to characterize a structural pattern and the corresponding decimal number of the binary coding is the LBP code of the center pixel [9].
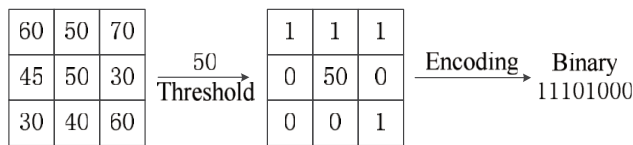
60	50	70
45	50	30
30	40	60

$\xrightarrow[\text{Threshold}]{50}$

1	1	1
0	50	0
0	0	1

$\xrightarrow{\text{Encoding}}$ Binary 11101000

FIGURE 3. The thresholding step and the encoding step of LBP.

LBP can be defined as follows:

$$LBP_{P,R} = \sum_{p=0}^{P-1} s(g_p - g_c)2^p, \quad s(x) = \begin{cases} 1, & x \ge 0 \\ 0, & x < 0 \end{cases} \quad (9)$$

where g_p is the pth pixel value, and g_c is the center value within the image patch.

4) MEDIAN BINARY PATTERN

The theory of MBP [17] is similar to that of LBP, but it uses the median of the pixel values in the image patch as the local threshold rather than that of the center pixel. This difference can improve the sensitivity and noise robustness of the LBP descriptor. In general, MBP can be defined as follows:

$$MBP_{P,R} = \sum_{p=0}^{P-1} s(g_p - g_m)2^p, \quad s(x) = \begin{cases} 1, & x \ge 0 \\ 0, & x < 0 \end{cases} \quad (10)$$

where g_m is the median value within the image patch.

5) ADAPTIVE MEDIAN BINARY PATTERN

In traditional texture descriptors such as the LBP and MBP, the selection of the threshold value is usually limited to a small region. However, a small window could miss the optimal threshold value and the important spatial information. In contrast, a larger window contains richer local texture information to obtain the optimal threshold value. Considering that a constant window size cannot handle all of the variations in an image, an adaptive window is needed to change the analysis area of each center pixel depending on certain criteria. The AMBP [18], [19] considers larger and adaptive analysis windows around the center pixel to compute the optimal local threshold.

Algorithm 1 Adaptive Median Binary Patterns (AMBP)

1: Input: Gray scale Image I; maximum analysis window k_{max}; patch size P
2: Output: AMBP image M
3: For all i, j do
4:: $k \leftarrow 1$
5: Repeat
6:     $S \leftarrow I[i - k : i + k, j - k : j + k]$
7:     $Z_{med} \leftarrow median(S)$
8:     $Z_{min} \leftarrow min(S)$
9:     $Z_{max} \leftarrow max(S)$
10:    If $Z_{min} + \alpha \cdot d < Z_{med} < Z_{max} - \alpha \cdot d$ then break
11:    $k \leftarrow k + 1$
12: Until $k \le k_{max}$
13: If $Z_{min} + \alpha \cdot d < I[i, j] < Z_{max} - \alpha \cdot d$ then
14:    $\tau = I[i, j]$
15: Else $\tau = Z_{med}$ (τ is the parameter used as the threshold value)
16: End if
17: $M[i, j] \leftarrow P - bit$ binary pattern
18: End

AMBP contains three stages: determination of the optimal size of analysis window, determination of the local threshold value and encoding. Algorithm 1 shows the process of AMBP.

Let $S(i, j)$ be the square analysis window around the given coordinates (i, j), and let x_c be the pixel value at this location. We define d as the magnitude of the difference between the center pixel and its neighbors, and it is related to the analysis window size.

$$d = \frac{1}{|S|} \sum_{m \in S(i,j)} |x_c - x_m|, \quad m \ne c \quad (11)$$

The testing condition of the optimal analysis window size is as follows:

$$Z_{min} + \alpha \cdot d < Z_{med} < Z_{max} - \alpha \cdot d \quad (12)$$

where α is a control parameter that determines the range of values for the median. If $\alpha = 0$, then the median value is limited between the minimum and maximum, which is the testing condition of the standard AMBP. If $\alpha \ne 0$, then the median range is related to d.

To obtain the optimal size of analysis window, we set a maximal window size and conduct a repetition. In each looped iteration, the median value of this square analysis window is tested to determine whether it meets the testing condition, which means whether it lies in the range $[Z_{\min} + \alpha \cdot d, Z_{\max} - \alpha \cdot d]$. If the median value doesn't meet this condition, then the window size is increased by two. This process is repeated until the value meets this condition or the maximal window size is reached.

After obtain the optimal window size, to determine the optimal local threshold value, if the center pixel lies in the range $[Z_{\min} + \alpha \cdot d, Z_{\max} - \alpha \cdot d]$, the center pixel is selected as the local threshold value, and otherwise, the median pixel is selected as the local threshold value.

It must be noted that the optimal size of analysis window is determined to seek the optimal threshold value. After the threshold steps, in the process of encoding, the AMBP value is encoded in the predefined encoding window as the following equation:

$$AMBP_{P,R} = \sum_{p=0}^{P-1} s(g_p - \tau)2^p, \quad s(x) = \begin{cases} 1, & x \geq 0 \\ 0, & x < 0 \end{cases} \quad (13)$$

where P is the defined patch size.

B. PROPOSED TEXTURE ANALYSIS METHOD: ADAPTIVE ROBUST BINARY PATTERN

In this work, we are interested in the hyphae and nerves in cornea images rather than the background. Considering that the brightness of the hyphae and nerves is higher than that of the background, we improve the AMBP by adding the average pixel value of the analysis window as a new parameter.

Similar to AMBP, the process of ARBP contains three steps: determination of the optimal size of the analysis window, determination of the local threshold value and encoding.

In contrast to AMBP, we add a new parameter Z_{para}. In the repetition to obtain the optimal analysis window size, to determinate the size that can extract more texture information about the hyphae and nerves with high pixel values, we select the parameter Z_{para} from Z_{ave} and Z_{med} which has the further distance from the center pixel value. If Z_{para} lies in the range $[Z_{\min} + \alpha \cdot d, Z_{\max} - \alpha \cdot d]$, then we break the repetition and obtain the optimal size, otherwise, the window size is increased by two. This process is repeated until the value meets this condition or the maximal window size is reached.

Then, after this repetition, if the center pixel lies in the range $[Z_{\min} + \alpha \cdot d, Z_{\max} - \alpha \cdot d]$, the center pixel is selected as the local threshold value, otherwise, Z_{para} is selected as the local threshold value. In the encoding steps, the same as in AMBP, The ARBP value is encoded in the predefined encoding window according to the following equation:

$$ARBP_{P,R} = \sum_{p=0}^{P-1} s(g_p - \tau)2^p, \quad s(x) = \begin{cases} 1, & x \geq 0 \\ 0, & x < 0 \end{cases} \quad (14)$$

Algorithm 2 shows this process. The newly proposed method is more robust in texture description than AMBP; therefore, it was termed the adaptive robust binary pattern (ARBP).

Algorithm 2 Adaptive Robust Binary Pattern (ARBP)

---
1 Input: Gray scale Image I; maximum analysis window $k_{\max}$; patch size P
2 Output: ARBP image M
3 For all i, j do
4 $k \leftarrow 1$
5 Repeat
6     $S \leftarrow I[i - k : i + k, j - k : j + k]$
7     $Z_{med} \leftarrow median(S)$
8     $Z_{\min} \leftarrow \min(S)$
9     $Z_{\max} \leftarrow \max(S)$
10     $Z_{ave} \leftarrow average(S)$
11     $d = \frac{1}{|S|} \sum_{m \in S(i,j)} |x_c - x_m|, m \neq c$
12   If $|Z_{med} - I[i,j]| < |Z_{ave} - I[i,j]|, Z_{para} = Z_{ave}$
13   Else $Z_{para} = Z_{med}$
14   If $Z_{\min} + \alpha \cdot d < Z_{para} < Z_{\max} - \alpha \cdot d$ then break
15     $k \leftarrow k + 1$
16 Until $k \leq k_{\max}$
17 If $Z_{\min} + \alpha \cdot d < I[i,j] < Z_{\max} - \alpha \cdot d$ then
18   $\tau = I[i, j]$
19 Else $\tau = Z_{para}$ (τ is the parameter used as the threshold value)
20 End if
21 $M[i, j] \leftarrow P - bit$ binary pattern
22 End

C. CLASSIFIER: SUPPORT VECTOR MACHINE

The support vector machine (SVM) [20] is a powerful supervised learning model in machine learning that can efficiently perform a non-linear classification by a kernel function. It is a pretty efficient method and works well in small sample problems because it can ensure the minimization of both the structure risk and the empirical error.

SVM convert the non-linear M-dimensional samples x with the label y into a K-dimensional feature space $(K > M)$ by the kernel function $\varphi(x)$ to realize linear separation.

The separation of two classes is performed by the hyperplane defined in equation (15)

$$\begin{cases} g(x) = w^T \varphi(x) + b \geq 1 \text{ if } y = 1 \\ g(x) = w^T \varphi(x) + b \leq -1 \text{ if } y = -1 \end{cases} \quad (15)$$

where $\varphi(x) = [\varphi_1(x), \varphi_2(x), \ldots, \varphi_k(x)]^T$ is a series of non-linear kernel functions, such as radial Gaussian basis, polynomial, spline, or sigmoid functions, $w = [w_1, w_2, \ldots w_k]^T$ is the weight vector of network, and b is the bias.

SVM computes the optimal classification parameter via minimization of the classification error and maximization of the separation margin between two classes. Mathematically, it corresponds to the minimization of the cost

function $\Phi(\omega, \xi)$ defined as

$$\min \ \Phi(w, \xi) = 1/2 w^T w + C \sum_{i=1}^{P} \xi_i$$

$$\text{subject to } y_i(w^T \varphi(x_i) + b) \geq 1 - \xi_i,$$

$$\xi_i \geq 0, \quad i = 1, 2, \ldots, p \quad (16)$$

where $C > 0$ is the user-specified constant that represents the regularization coefficient, p is the number of given learning data pairs x_i, y_i, and $\xi_i \geq 0$ is the nonnegative slack variable.

It is easy to prove [27] that, for the optimal hyperplane,

$$w = \sum_{i=1}^{P} \alpha_i y_i \varphi(x_i) \quad (17)$$

where α_i are positive real numbers that satisfies:

$$\max \ Q(\alpha) = \sum_{i=1}^{P} \alpha_i - \sum_{i=1}^{P} \sum_{j=1}^{P} \alpha_i \alpha_j d_i d_j \langle \varphi(x_i), \varphi(x_j) \rangle$$

$$\text{subject to } \sum_{i=1}^{P} a_i y_i = 0, \quad a_i > 0 \quad (18)$$

The decision function can equivalently be expressed as

$$g(x) = sign(\sum_{i=1}^{P} \alpha_i y_i \langle \varphi(x_i), \varphi(x) \rangle - b) \quad (19)$$

D. CLASSIFICATION FRAMEWORK

The classification framework in this paper includes three steps: image enhancement, texture feature extraction and classification.

First, because of the restrictive conditions in the image acquisition process and the complex environment of the ocular surface, the cornea images have a messy background and many noise pixels [9]. Thus, image enhancement is needed to enhance the targets before feature extraction. The brightness of the images is uneven, and thus, a contrast stretching algorithm [28] applied to the sub-parts with different brightness could lead to inaccurate enhancement. To solve this problem, a sub-regional contrast stretching algorithm is applied. The whole image is divided into $M * N$ sub-rectangle areas, and every sub-rectangle has relatively even background. The stretching parameters are set dynamically according the gray level in each sub-rectangle.

Then, the newly proposed texture analysis method ARBP is used to extract the texture features of the cornea images. We calculate the ARBP value of every pixel and obtain the ARBP feature, which is still an image. We consider the statistical histogram of the ARBP feature image as the final feature vector. The statistical histogram that describes the frequency of every ARBP value is a typical representative of the original ARBP feature image.

Lastly, we train the SVM classifier with the extracted ARBP feature vectors and the labels of cornea images. The SVM classifier is implemented by LIBSVM [29], and the

kernel function is RBF function because of its excellent classification results. During the training processing, the penalty parameters and kernel parameters in SVM are determined via cross-validation.

IV. HYPHAE DETECTION AND QUANTITATIVE EVALUATION

After the classification, the images are divided into two classes, normal cornea images with nerve and abnormal cornea images with hyphae. In this section, we detect and measure the hyphae in the abnormal images. First, we preprocess the images and convert them to binary images; then, we detect hyphae using the line detection method LSD; finally, we define the hyphal density to quantitative evaluate the infection severity.

A. IMAGE PREPROCESSING

After applying the sub-regional contrast stretching algorithm in section III, the gray level difference between the background and targets, including hyphae and nerves, is much larger. To further separate the targets from the background, we convert the images into binary images, and Otsu's [30] method is used to obtain an optimal threshold for the binary image. Then, there are some small non-target areas in the binary images, and thus, we omit some connected domain areas that are smaller than the set size to remove the messy background and noise points.

B. HYPHAE DETECTION

Considering that hyphae are threads, we detect them using line detection. LSD is a linear-time line segment detector proposed by von Gioi [31] in 2012 based on the Burns, Hanson, and Riseman method [32], and it uses a contrario validation approach according to Desolneux, Moisan and Morel's theory [33], [34]. LSD is designed to be used on any digital image without parameter tuning. It controls for the number of false detections. On average, one false alarm is allowed per image.

The LSD algorithm inputs a gray-level image and returns a list of detected line segments. Briefly, LSD comprises calculation of the level line of each pixel to generate a level-line area. The vector and the level line are tangential. Thus, the area is divided into several connecting areas called line support regions. Each line support region is a candidate for a line segment, and a rectangle must be associated with it. The principal inertial axis of the line support region is used as the main rectangle direction, and the rectangle must cover the full region. The final line segments are selected from those line support regions according to certain criteria.

C. QUANTITATIVE EVALUATION OF THE INFECTION SEVERITY

To obtain a better understanding of hyphae detection and provide doctors diagnostic assistance, the infection severity must be quantitatively evaluated. In clinical diagnosis, doctors observe the number, length and morphological

features of hyphae using confocal microscopy to gain an understanding of the patient's infection status [8]. On this basis, the evaluation in this paper is made based on the line detection results, and we define the hyphal density (the length of the hyphae/unit area) of the fundus fungi as a measure of the infection severity. The higher the density is, the more severe the infection is.

From a clinical point of view, the diagnosis of fungal keratitis is a comprehensive judgment [3]. Doctors should consider patients' symptoms and the results of several medical examinations to determine a definite diagnosis. The hyphal density in this paper also acts as an auxiliary diagnosis factor to assist doctors in making a comprehensive diagnosis, rather than the decisive determinant of whether the patient has fungal keratitis.

V. EXPERIMENTAL RESULTS AND ANALYSIS

A. EXPERIMENTAL DATABASE

In this paper, the database comprises 183 normal images and 195 abnormal images, which were collected in vivo using Heidelberg Engineering HRT-3 confocal microscopy. The size of these images is 384×384.
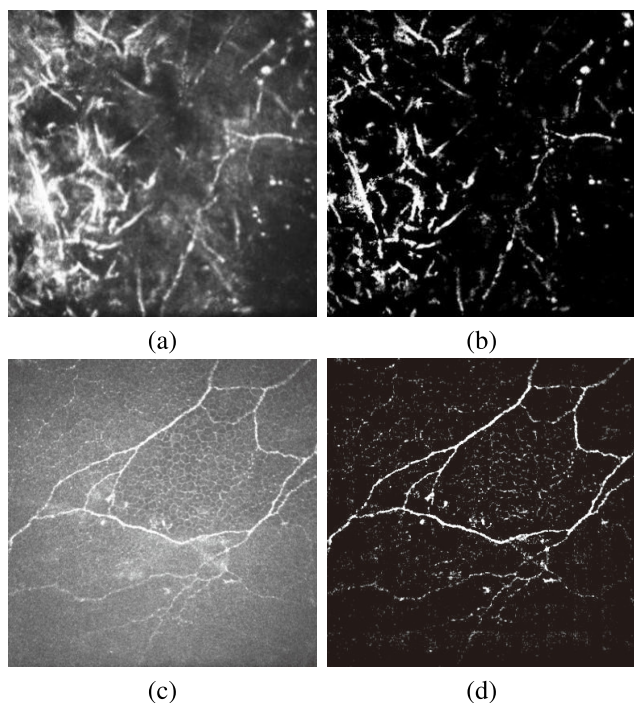

FIGURE 4. Image preprocessing results. (a) The original abnormal image. (b) The abnormal image after a sub-regional contrast stretching algorithm. (c) The original normal image. (d) The normal image after a sub-regional contrast stretching algorithm.

B. CLASSIFICATION RESULTS OF CORNEA IMAGES

After image enhancement using an $11 * 11$ sub-regional contrast stretching algorithm (see Fig. 4), we applied several texture analysis methods to extract texture features, including GLCM, Gabor, LBP, AMBP and the newly proposed

ARBP. In order to obtain the most excellent classification performance, several classifiers, including decision tree [35], K-nearest neighbour (KNN) [36], logistic regression [37] and SVM, are trained based on the above-mentioned texture features.

In this experiment, 10-fold cross validation was adopted to test the performance of the texture classification framework. What's more, the average accuracies of the classifiers were calculated by repeating the experiments 100 times.

In order to evaluate the performance of different texture analysis methods, we drew the receiver operating characteristic (ROC) diagram [38] and calculated the sensitivity *TPR*, specificity *TNR*, accuracy *ACC* and the area under *ROC* curve *AUC*, which are defined as follows:

$$TPR = TP/(TP + FN) \tag{20}$$

$$TNR = TN/(TN + FP) \tag{21}$$

$$ACC = (TP + TN)/(TP + FP + TN + FN) \tag{22}$$

$$AUC = \int_{-\infty}^{\infty} TPR(T)FPR'(T)dT \tag{23}$$

where *TP* is the number of true positive samples, *FP* is the number of false positive samples, *TN* is the number of true negative samples, and *FN* is the number of false negative samples, and $FPR = 1 - TNR$.

Sensitivity measures the proportion of positive samples that are correctly classified, and high sensitivity means a low missed diagnosis rate. Specificity measures the proportion of negative samples that are correctly identified, and high specificity means a low misdiagnosis rate. *ACC* measures the proportion of all of the samples that are correctly identified, and high classification *ACC* means a high classification accuracy. *AUC* calculates the area under *ROC* curve, and high *AUC* means excellent classification performance.

The *ROC* curve plots the true positive rate *TPR* against the false positive rate *FPR*. *ROC* illustrates the diagnostic ability of a binary classifier system while its discrimination threshold is varied. The best possible classification method would yield the point (0, 1) of the *ROC* space, which represents 100% sensitivity and 100% specificity [38]. The larger *AUC* is, the better the classification performance is.

TABLE 1. Experimental results of multiple classifiers using GLCM features.

Method	TPR (%)	TNR (%)	ACC (%)	AUC
DT	86.67	89.62	87.56	0.9603
KNN	78.46	87.43	81.67	0.8574
LR	98.46	98.91	98.07	0.9837
SVM	90.77	89.62	90.69	0.9071

The classification experimental results of several classifiers based on the above-mentioned features are shown in Table 1 - Table 5 , the ROC diagrams are shown in Fig. 5 - Fig. 9. Based on considerations on various factors including *TPR*, *TNR*, *ACC* and *AUC*, SVM classifier obtained almost the excellent classification performance based on the several
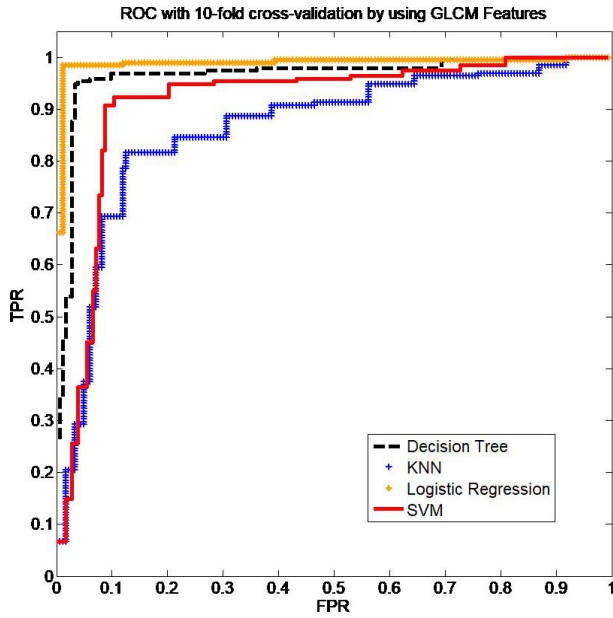
FIGURE 5. ROC curves of multiple classifiers using GLCM features by using the 10-fold cross validation.

TABLE 2. Experimental results of multiple classifiers using GABOR features.

Method	TPR (%)	TNR (%)	ACC (%)	AUC
DT	89.74	90.16	91.51	0.9303
KNN	99.49	90.17	95.64	0.9604
LR	97.44	98.36	97.46	0.9733
SVM	94.87	97.27	96.35	0.9617

TABLE 3. Experimental results of multiple classifiers using LBP features.

Method	TPR (%)	TNR (%)	ACC (%)	AUC
DT	74.36	72.13	78.01	0.8058
KNN	64.10	98.36	80.82	0.8419
LR	65.64	64.48	67.38	0.6760
SVM	92.82	96.17	95.11	0.9581

TABLE 4. Experimental results of multiple classifiers using AMBP features.

Method	TPR (%)	TNR (%)	ACC (%)	AUC
DT	97.44	95.63	96.83	0.9700
KNN	94.87	95.63	95.16	0.9468
LR	94.36	98.36	96.03	0.9558
SVM	97.44	97.81	97.36	0.9662

TABLE 5. Experimental results of multiple classifiers using ARBP features.

Method	TPR (%)	TNR (%)	ACC (%)	AUC
DT	100.00	99.45	99.71	0.9925
KNN	100.00	99.45	99.74	0.9940
LR	100.00	99.45	99.73	0.9934
SVM	100.00	99.45	99.74	0.9931

FIGURE 6. ROC curves of multiple classifiers using Gabor features by using the 10-fold cross validation.

FIGURE 7. ROC curves of multiple classifiers using LBP features by using the 10-fold cross validation.

TABLE 6. Experimental results of multiple features using SVM classifier.

Method	TPR (%)	TNR (%)	ACC (%)	AUC
GLCM	90.77	89.62	90.69	0.9071
Gabor	94.87	97.27	96.35	0.9617
LBP	92.82	96.17	95.11	0.9581
AMBP	97.44	97.81	97.36	0.9662
ARBP	100.00	99.45	99.74	0.9901

above-mentioned features. Therefore, we adopted SVM classifier in this classification framework to compare different texture feature descriptors.
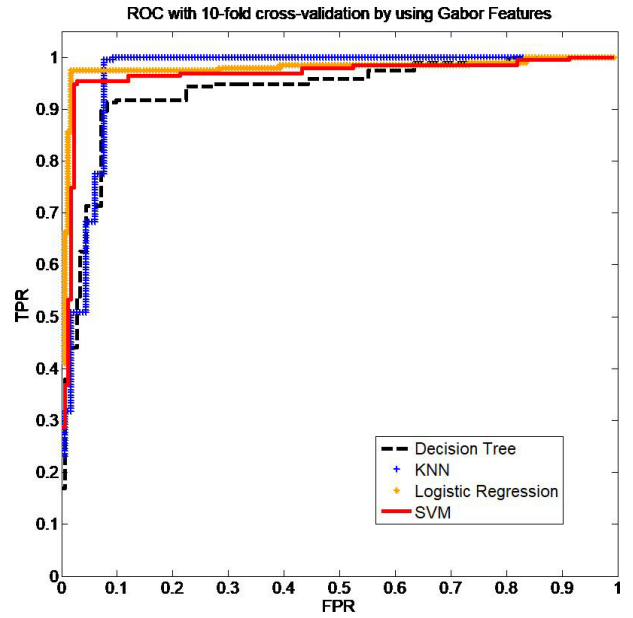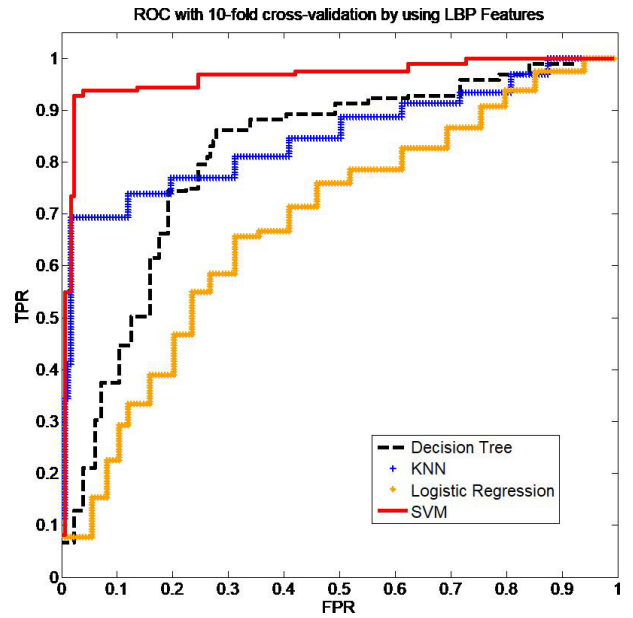
The classification experimental results of different texture feature descriptors based on SVM classifier are shown in Table 6, and the ROC diagram is shown in Fig. 10. As can
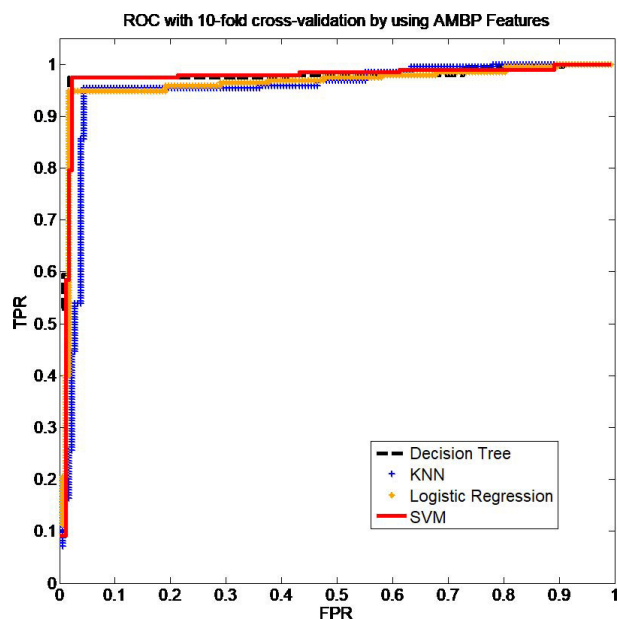
FIGURE 8. ROC curves of multiple classifiers by using AMBP features using the 10-fold cross validation.
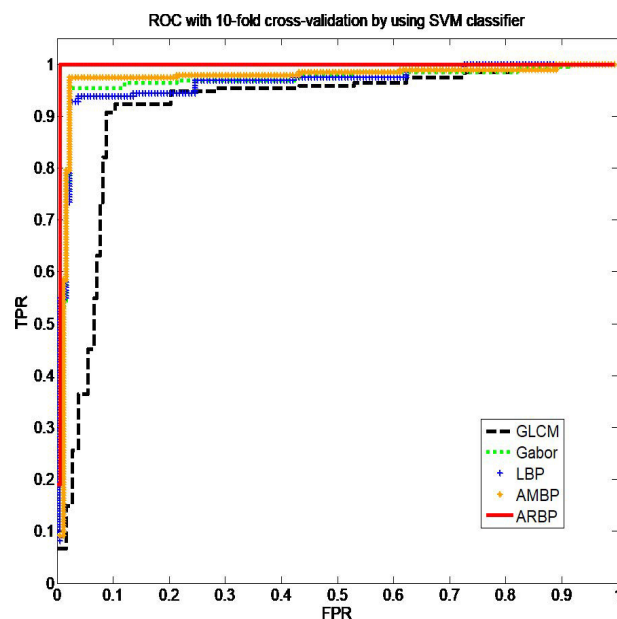

FIGURE 9. ROC curves of multiple classifiers using ARBP features by using the 10-fold cross validation.

FIGURE 10. ROC curves of multiple features using SVM classifier using the 10-fold cross validation.
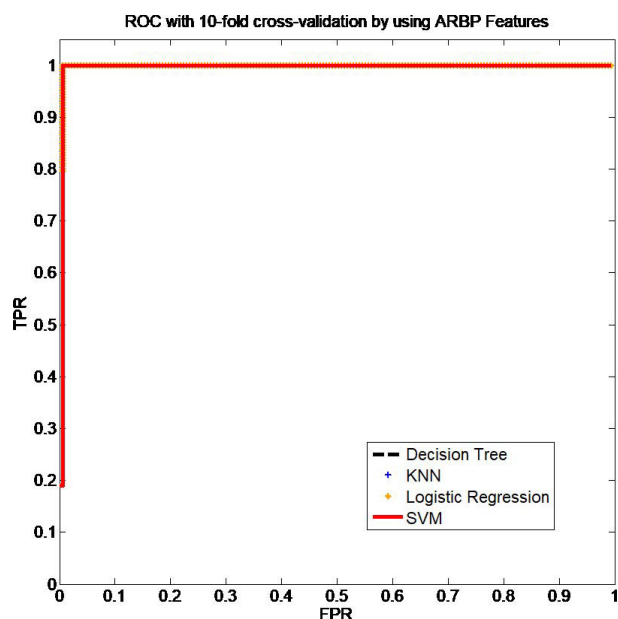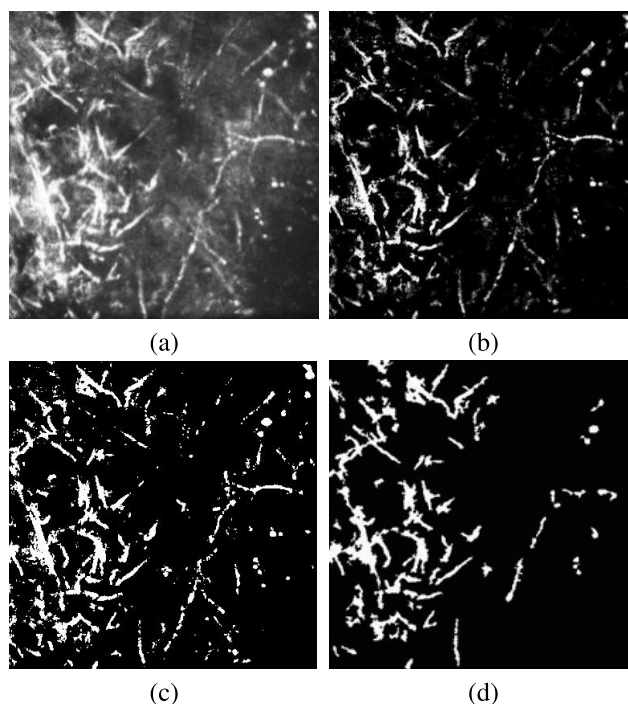

FIGURE 11. Image preprocessing results. (a) The original abnormal image. (b) The image after a sub-regional contrast stretching algorithm. (c) Binary image with the threshold determined using Otsu's method. (d) Image after the connected domain process.

been see, all of the texture analysis methods can achieve accuracies in excess of 90%. For the traditional texture analysis methods, the classification performances of Gabor and LBP are almost similar, which are better than that of GLCM and slightly worse than that of AMBP. The newly proposed ARBP obtained the most excellent classification performance compared with the other methods, it could perfectly separate the abnormal cornea images from normal cornea images with the accuracy of 99.74%, and the values of *TPR*, *TNR*, *AUC* are close to 1. Furthermore, the *ROC* curve of ARBP is close to the best possible *ROC* curve. These experimental results

demonstrate the effectiveness of the proposed classification framework.

C. RESULTS OF HYPHAE DETECTION AND QUANTITATIVE EVALUATION

We preprocessed the images and converted them to binary images, and the preprocessing results are shown in Fig. 11.
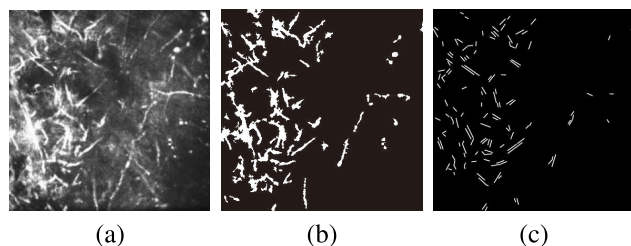
Afterward, we detected the hyphae using the LSD algorithm. As shown in Fig. 12, most of the hyphae have been effectively detected as short lines.
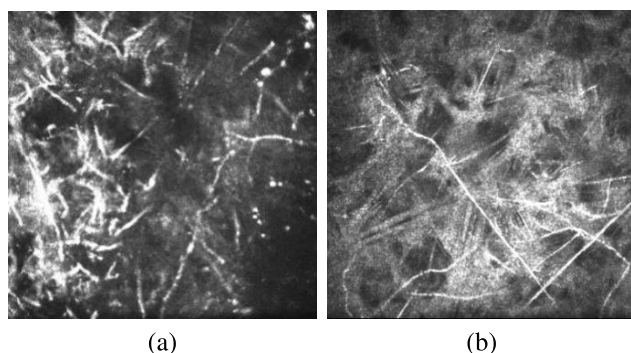

FIGURE 13. Hyphal density calculation results (a) A hyphal density of 1875. (b) A hyphal density of 1570.

We calculated the hyphal density of the abnormal hyphae images using the ratio of length versus area. Considering that all of the test images have the same area, the hyphal density can be represented by the lengths of the hyphae. Fig. 13 shows the results for two hyphae images. The former has a hyphal density of 1875, and the latter has a density of 1570, which means that the first patient has a higher possibility of having a severer fungal keratitis. The evaluation result can provide doctors with auxiliary diagnostic information and assist doctors in combining the patient's symptoms and the results of several other medical examinations to determine a diagnosis.

VI. CONCLUSIONS AND FUTURE RESEARCH

In this study, a novel framework for detecting and measuring hyphae is proposed. We classify normal and abnormal images based on the newly proposed texture analysis method adaptive robust binary pattern (ARBP) and the classic classifier support vector machine (SVM), and then, we preprocess the abnormal images to enhance the targets and use the line segment detector (LSD) algorithm to detect the hyphae. Furthermore, the hyphal density is defined to quantitatively evaluate the infection severity. The experimental results demonstrate the effectiveness of the proposed framework. The newly proposed adaptive robust binary pattern (ARBP) can help extract

effective texture features of images with relatively bright and small targets.

We aimed to establish an intelligent confocal images analysis and diagnosis system to provide doctors with auxiliary diagnostic information. There are several species of fungi with different forms that can lead to fungal keratitis, such as fusarium and aspergillus. At the present stage, we have implemented two-class classification, respectively, abnormal images and normal images. Further more, we need to extract deeper texture features and implement classification of different fungi that present different forms. To achieve this goal, first and most importantly, we must collect a very large number of images of corneas infected by different fungi. Then we plan to introduce deep learning methods to the feature extraction and classification of the cornea images, such as convolution neural network and deep belief network. Establishing an intelligent confocal images analysis and diagnosis system is a large challenge, although at present it cannot replace doctors in making a medical diagnosis, we believe that as the rapid renovation and industrialization of technique, intelligent medical images analysis and diagnosis system will provide doctors increasingly accurate diagnostic messages and convenient services.

REFERENCES

[1] L. Xie, W. Zhong, W. Shi, and S. Sun, "Spectrum of Fungal Keratitis in North China," *Ophthalmology*, vol. 113, pp. 1943–1948, Nov. 2006.

[2] M. Li and L. Zhang, "Research advance of fungal keratitis," *Int. J. Ophthalmol.*, vol. 8, no. 2, pp. 384–387, Feb. 2008.

[3] S. Belliappa, J. Hade, S. Kim, B. D. Ayres, and D. S. Chu, "Surgical outcomes in cases of contact lens-related fusarium keratitis," *Eye Contact Lens.*, vol. 36, pp. 190–194, Jul. 2010.

[4] L. Xie, H. Zhai, J. Zhao, S. Sun, W. Shi, and X. Dong, "Antifungal susceptibility for common pathogens of fungal keratitis in Shandong Province, China," *Amer. J. Ophthalmol.*, vol. 146, no. 2, pp. 260–265, Aug. 2008.

[5] S. H. Khairallah, K. A. Byrne, and K. F. Tabbara, "Fungal keratitis in Saudi Arabia," *Document. Ophthalmol.*, vol. 79, no. 3, pp. 269–276, 1992.

[6] M. A. Dahlgren, A. Lingappan, and K. R. Wilhelmus, "The clinical diagnosis of microbial keratitis," *Amer. J. Ophthalmol.*, vol. 143, no. 6, pp. 940–944, Jun. 2007.

[7] J. B. Pawley, "Handbook of biological confocal microscopy," *J. Biomed. Opt.*, vol. 25, no. 3, p. 029902, Jan. 1995.

[8] G. J. Florakis, G. Moazami, H. Schubert, C. J. Koester, and J. D. Auran, "Scanning slit confocal microscopy of fungal keratitis," *Arch. Ophthalmol.*, vol. 115, pp. 1461–1463, Nov. 1997.

[9] Q. Qiu, Z. Liu, Y. Zhao, D. Wei, and X. Wu, "Automatic detecting cornea fungi based on texture analysis," presented at the IEEE Int. Conf. Smart Cloud, Nov. 2016.

[10] X. Xie and M. Mirmehdi, "A galaxy of texture features," in *Handbook of Texture Analysis*. London, U.K.: Imperial College Press, 2008, pp. 375–406.

[11] F. Riaz, A. Hassan, S. Rehman, and U. Qamar, "Texture classification using rotation- and scale-invariant gabor texture features," *IEEE Signal Process. Lett.*, vol. 20, no. 6, pp. 607–610, Jun. 2013.

[12] L. S. Davis, S. A. Johns, and J. K. Aggarwal, "Texture analysis using generalized co-occurrence matrices," *IEEE Trans. Pattern Anal. Mach. Intell.*, vol. PAMI-1, no. 3, pp. 251–259, Jul. 1979.

[13] V. Cherkassky, "The nature of statistical learning theory," *IEEE Trans. Neural Netw.*, vol. 8, no. 6, p. 1564, Nov. 1997.

[14] D. A. Clausi and H. Deng, "Design-based texture feature fusion using Gabor filters and co-occurrence probabilities," *IEEE Trans. Image Process.*, vol. 14, no. 7, pp. 925–936, Jul. 2005.

[15] T. Ojala, K. Valkealahti, E. Oja, and M. Pietikäinen, "Texture discrimination with multidimensional distributions of signed gray-level differences," *Pattern Recognit.*, vol. 34, no. 3, pp. 727–739, 2001.

[16] L. Liu, Y. Long, P. W. Fieguth, S. Lao, and G. Zhao, "BRINT: Binary rotation invariant and noise tolerant texture classification," *IEEE Trans. Image Process.*, vol. 23, no. 7, pp. 3071–3084, Jul. 2014.

[17] A. Hafiane, G. Seetharaman, K. Palaniappan, and B. Zavidovique, "Rotationally invariant hashing of median binary patterns for texture classification," presented at the Int. Conf. Image Anal. Pattern Recognit., 2008.

[18] A. Hafiane, K. Palaniappan, and G. Seetharaman, "Adaptive median binary patterns for texture classification," presented at the Int. Conf. Pattern Recognit., Aug. 2014.

[19] A. Hafiane, K. Palaniappan, and G. Seetharaman, "Joint adaptive median binary patterns for texture classification," *Pattern Recognit.*, vol. 48, no. 8, pp. 2609–2620, Aug. 2015.

[20] M. M. Adankon and M. Cheriet, "Support vector machine," presented at the Int. Conf. Intell. Netw. Intell. Syst., Nov. 2009.

[21] V. Gaike, R. Mhaske, S. Sonawane, N. Akhter, and P. D. Deshmukh, "Clustering of breast cancer tumor using third order GLCM feature," presented at the IEEE Int. Conf. Green Comput. Internet Things, Oct. 2016.

[22] S. Rohini and S. Soma, "A novel texture based skin melanoma detection using color GLCM and CS-LBP feature," *Int. J. Comput. Appl.*, vol. 171, no. 5, pp. 1–5, Aug. 2017.

[23] R. Rastghalam and H. Pourghassem, "Breast cancer detection using MRF-based probable texture feature and decision-level fusion-based classification using HMM on thermography images," *Pattern Recognit.*, vol. 51, pp. 176–186, Mar. 2016.

[24] A. Ahmadvand and M. R. Daliri, "Improving the runtime of MRF based method for MRI brain segmentation," *Appl. Math. Comput.*, vol. 256, pp. 808–818, Apr. 2015.

[25] Z. Zou, J. Yang, V. Megalooikonomou, R. Jennane, E. Cheng, and H. Ling, "Trabecular bone texture classification using wavelet leaders," presented at the SPIE Med. Imag., vol. 9788. Mar. 2016, p. 97880E.

[26] J. Virmani, "Breast tissue density classification using wavelet-based texture descriptors," in *Proc. 2nd Int. Conf. Comput. Commun. Technol.*, Sep. 2016, pp. 539–546.

[27] T. S. Furey, N. Cristianini, N. Duffy, D. W. Bednarski, M. Schummer, and D. Haussler, "Support vector machine classification and validation of cancer tissue samples using microarray expression data," *Bioinformatics*, vol. 16, no. 10, pp. 906–914, 2000.

[28] C.-C. Yang, "Image enhancement by modified contrast-stretching manipulation," *Opt. Laser Technol.*, vol. 38, no. 3, pp. 196–201, Apr. 2006.

[29] C.-C. Chang and C.-J. Lin, "LIBSVM: A library for support vector machines," *ACM Trans. Intell. Syst. Technol.*, vol. 2, no. 3, pp. 1–27, Jul. 2012.

[30] N. Otsu, "A threshold selection method from gray-level histograms," *IEEE Trans. Syst., Man, Cybern.*, vol. 9, no. 1, pp. 62–66, Jan. 1979.

[31] R. G. von Gioi, J. Jakubowicz, J.-M. Morel, and G. Randall, "LSD: A fast line segment detector with a false detection control," *IEEE Trans. Pattern Anal. Mach. Intell.*, vol. 32, no. 4, pp. 722–732, Apr. 2008.

[32] J. B. Burns, A. R. Hanson, and E. M. Riseman, "Extracting straight lines," *IEEE Trans. Pattern Anal. Mach. Intell.*, vol. PAMI-8, no. 4, pp. 425–455, Jul. 1986.

[33] A. Desolneux, L. Moisan, and J.-M. Morel, "Meaningful alignments," *Int. J. Comput. Vis.*, vol. 40, no. 1, pp. 7–23, Oct. 2000.

[34] A. Desolneux, L. Moisan, and J.-M. Morel, "From gestalt theory to image analysis: A probabilistic approach," *Interdiscipl. Appl. Math.*, vol. 34, no. 3, pp. 1255–1259, 2008.

[35] J. R. Quinlan, "Induction of decision trees," *Mach. Learn.*, vol. 1, no. 1, pp. 81–106, 1986.

[36] S. A. Dudani, "The distance-weighted k-nearest-neighbor rule," *IEEE Trans. Syst., Man, Cybern., Syst.*, vol. SMC-6, no. 4, pp. 325–327, Apr. 1976.

[37] C. Andrew, "Applied logistic regression," *Technometrics*, vol. 34, no. 3, pp. 358–359, Mar. 2000.

[38] M. Grzybowski and J. G. Younger, "Statistical methodology: III. Receiver operating characteristic (ROC) curves," *Academic Emerg. Med.*, vol. 4, no. 8, pp. 818–826, 1997.

XUELIAN WU is currently pursuing the Ph.D. degree with Shandong University. She is specialized in intelligent medical image analysis and the treatment of cataract and ocular surface disorders.

QINGCHEN QIU is currently pursuing the M.S. degree with the School of Information Science and Engineering, Shandong University, Jinan, China. Her research interests include image processing and pattern recognition.

ZHI LIU received the Ph.D. degree from the Institute of Image Processing and Pattern Recognition, Shanghai Jiao Tong University, in 2008. He is currently an Associate Professor with the School of Information Science and Engineering, Shandong University. He is the Head of the Intelligent Information Processing Group. His current research interests include the applications of computational intelligence to linked multicomponent big data systems, medical images in the neurosciences, multimodal human-computer interaction, remote sensing image processing, content-based image retrieval, semantic modeling, data processing, classification, and data mining.

YUEFENG ZHAO received the Ph.D. degree from the Anhui Institute of Optics and Fine Mechanics, Chinese Academy of Sciences. He is currently the Vice Professor with the School of Physics and Electronics, Shandong Normal University. His current research interests include raman gain lidar to detect the tropospheric carbon dioxide concentration.
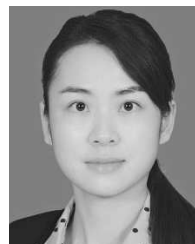
BIN ZHANG is currently a Physician of ophthalmology with the Shandong Provincial Maternity and Child Care Hospital. She specializes in the treatment of various types of pediatric ophthalmic diseases, such as newborn corneal disease, ametropia, strabismus, and amblyopia.

YONG ZHANG is currently the Deputy Director of the physicians of ophthalmology with the Shandong Provincial Hospital of Ophthalmology, where he is involved in the pathology and clinical protocols of excimer lasers for the treatment of ametropia. He specializes in excimer lasers for the treatment of ametropia, phacoemulsification and corneal transplants.

XINYI WU is currently the Chief Physician of ophthalmology, a Ph.D. Supervisor, and the Director of the Department of Ophthalmology, Qilu Hospital of Shandong University. She specializes in the treatment of various types of complex ophthalmic diseases, such as corneal disease, cataracts, and ocular surface disease.

JIANMIN REN is currently the Chief Physician and a Master's Student Supervisor with the Qilu Hospital of Shandong University.

● ● ●